DOI: 10.24352/UB.OVGU-2018-006 TECHNISCHE MECHANIK, 38, 1, (2018), 55 – 72
submitted: August 1, 2017

Modeling of Aging Effects in a Zinc Die Casting Alloy

M. A. Martinez Page, S. Hartmann

Zinc die casting alloys, also known as zamak, are widely used to produce components of cars and machines. Because of their low melting point and their ability to produce very accurate components, these alloys are considered to be the best castable of all commonly used alloys. This advantage is accompanied by a pronounced rate dependence and aging. In this work, we investigate these effects at room temperature for the zinc die casting alloy zamak 5 using tension, compression and torsion experiments. A three-dimensional constitutive model of small strain viscoplasticity is proposed, in which the aging is included by an internal variable. The model is calibrated to the experimental data. In this point, the partitioned structure of the model plays an important role. Moreover, the stress algorithm of the model is shown and finite element simulations are carried out to show the behavior of the model.

1 Introduction

Aging denotes the development of the material properties and mechanical response due to microstructural changes in the course of time. These changes are associated with precipitation of alloying elements or phases with low solubility, phase decomposition, and changes in the crystallographic structure. An increment in temperature generates changes in solid solubility, which can accelerate the process, see, for example, (Callister and Rethwisch, 2016). In polymers, aging can also be associated to physical or chemical changes, see (Lion and Johlitz, 2012) and the literature cited therein. If it is not considered, aging effects can imply an overestimation (or underestimation) of the mechanical response of a component part, which can conduce to its failure.

Zamak alloys consist of zinc as the basis metal, a constant amount of 4% aluminum, and, furthermore, magnesium and copper as alloying elements. They are commonly used in components for cars and machines because of its castability, its mechanical properties, and its economical price. Because of its low melting point of $380\,^{\circ}\mathrm{C}$, zamak undergoes a strong aging process even at room temperature. From the point of view of Material Science, there are some investigations which describe microstructural changes during aging in zinc alloys. Studies on zinc-aluminum alloys can be found in (Murray, 1983). In (Johnen, 1981), the die-casting process is explained and some general technical information about zinc die-cast alloys is given. Additionally, it is mentioned that zinc die-cast alloys tend to show a reduction in their dimensions in the course of time (shrinkage). There are also studies focusing on other aspects such as the creep behavior, the aging, and the consequent volume changes as well as the inter-crystalline corrosion. In the works of Gebhard (1940, 1942), the structure and different phases of the Zn-Al-Cu alloys as well as their volume changes are investigated. Gebhard (1941) treated the decomposition of the aluminum-rich β-phase in Zn-Al alloys. According to Gebhard (1942) and Kallien and Busse (2009), there are different mechanisms during the aging process that produce volume changes. On one hand, there are phase transformations such as the decomposition of the fcc β-crystal phase, the solid phase transformation of the β-, zinc-rich η-, copper-rich ε- and the ternary compound T-phases, and the precipitation of some elements that were diluted in the mix-crystals. On the other hand, there are volume changes in alloys which are in the η-T-β'-area because of changes in the concentration. Additional metastable phases are recognized in (Zhu, 2001; Zhu et al., 2002, 2003) – while a general rule of phase decomposition for Zn-Al based alloys is given in (Zhu, 2004). In (Kallien and Busse, 2009) and (Leis and Kallien, 2011), different zamak alloys are investigated, including the analysis of their aging mechanisms. Moreover, the influence of the temperature, the natural and artificial aging, the thickness of the specimens and the casting conditions on several mechanical parameters are shown.

The modeling of aging was treated in several works. The definition of aging as exposed by Krempl (1979) is adopted by Marquis and Lemaitre (1988). Aging is regarded as a modification of the micro-structure in such a way that the same loading process – performed in the same environment at different times (or ages of the material) – will lead to different mechanical responses. In (Marquis and Lemaitre, 1988) a model to couple elasto-plasticity,

damage, and aging for small deformations is proposed. Marquis and Costa Mattos (1991) provided a model for plasticity and aging. In both models, the effects of aging are represented by a new internal variable. Carol and Bazant (1993) suggested a model of viscoelasticity to account for aging of concrete in terms of an integral involving the relaxation function of the non-aging constituent and the variable volume fraction of the solidified constituent. A three-dimensional multisurface viscoplasticity model, which is proposed by (Meschke, 1996) is able to represent the time-dependent behavior of shotcrete. In that work, the aging is modeled by an additional part of the strain tensor. Bazant and Huet (1999) suggested an integral form for aging viscoelasticity without internal variables. Moreover, there are models for polymers, such as in (Maghous and Creus, 2003), where a homogenized thermoviscoelasticity model with aging is shown. Johlitz (2012) distinguishes between chemical and physical aging in polymers and develops a model for small deformations in which the aging is represented by internal variables as well. In (Johlitz and Lion, 2013; Johlitz and Diercks, 2014; Lion and Johlitz, 2012), a chemo-thermochemical and a chemical aging model for elastomers for small deformations is proposed and Dippel et al. (2014) proposed a solution for polymer bonds at large deformations. Most of these models are not able to describe volume changes due to aging.

In this work, we investigate the rate-dependent effects and the influence of aging in a zinc die casting alloy. The article is divided into five main sections. Firstly, experiments in thin-walled cylindrical tubes of zamak 5 at different strain rates and aging times are performed to investigate the changes in the mechanical response due to aging stage. Based on these experiments, a model of viscoplasticity is developed, where the aging is described with an aging variables. Subsequently, the model is calibrated to the experimental data. For calibrating the aging variable, measurements from Gebhard (1942) are taken into account as well. Finally, the stress algorithm of the model is shown, and finite element simulations are performed, where the rate dependence and the aging effect are shown.

2 Experimental Work

The characterization of the mechanical response of zamak 5 (ZnAl4Cu1) is carried out with tension, compression and torsion tests. The chosen specimen's geometry is a hollow cylinder with an inner radius of $R_i = 13\,\mathrm{mm}$, a wall thickness of $d = 2\,\mathrm{mm}$, and a length of $L = 90\,\mathrm{mm}$. For the treatment of the experimental data, it is reasonable to assume that the tube is thin-walled and that the stress state of the specimen is homogeneous in the middle region. The deformation and stress in tension and compression tests are calculated from the measurements by $\varepsilon = (L_e - L_0)/L_0$ and $\sigma = F/A$, where $L_0 = 20\,\mathrm{mm}$ and L_e are the initial and current length of the applied extensometer, which was placed in the middle of the specimen. The measured force is defined by F and the initial cross section $A = \pi(R_o^2 - R_i^2)$, with the outer radius $R_o = R_i + d$. For the torsion experiments, in case of a thin-walled tube, the shear strain γ and shear stress τ can be calculated by $\gamma = R_m(\tan\varphi)/L \approx (\varphi R_m)/L$ and $\tau = M_T/(2dA_m)$, with the mean radius $R_m = R_i + d/2$ and the length of the specimen L between the testing machine clemps. φ is the rotation angle, M_T the measured torque, and $A_m = \pi R_m^2$ is the area of the circle with the radius R_m.

The investigations of aging draw on natural aging. In order to investigate the effect of aging on the mechanical response, first, specimens without aging were tested, and, subsequently, tests were performed at three different aging times of 3, 6 and 12 months. In order to obtain "correct" ages, the specimens were stored in a freezer at the temperature of $-24\,^{\circ}\mathrm{C}$ in order to prevent undesired aging of the material. At this temperature, the material would need 100 years to age, see (Kallien and Busse, 2009).

2.1 Viscoplastic Behavior

The first investigations concentrate on the rate dependence. The goal is to characterize of the main behavior of the material and are carried out with unaged specimens. In a second step, the influence of aging is investigated.

2.1.1 Rate-dependence

First, the rate-dependent material behavior is investigated. To this end, tension, compression and torsion tests at four different strain rates were carried out. These strain rates differ from each other in one order of magnitude. We chose $\dot{\varepsilon}_k = 3.3 \times 10^{-k}\mathrm{s}^{-1}$, $k = 4, 5, 6, 7$ for tension and compression tests. For the shear tests, we defined $\dot{\gamma}_k = 3.2 \times 10^{-k}\mathrm{s}^{-1}$, $k = 4, 5, 6, 7$. In Figure 1 the results of these experiments are presented. As can be seen in

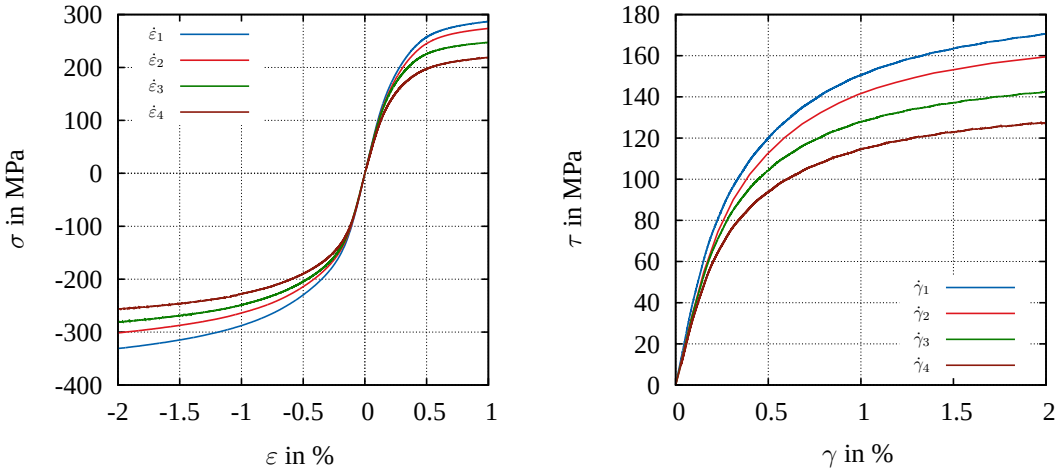

(a) Rate-dependence in tension/compression

(b) Rate-dependence in torsion

Figure 1. Results of the experiments at different strain rates

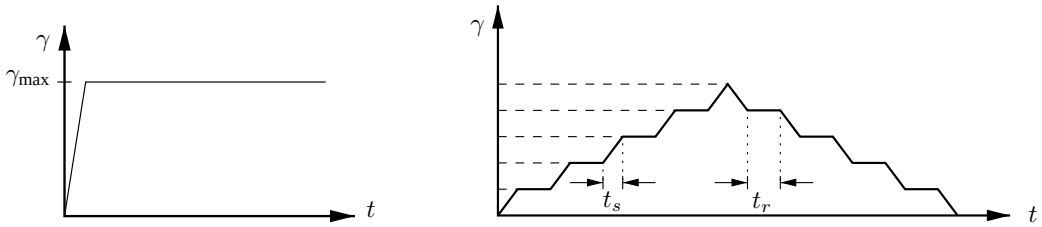

(a) Strain-path of the long time relaxation test

(b) Strain-path of the multistep relaxation test

Figure 2. Experiments for the estimation of the equilibrium state

the graphs, the compression and torsion tests were carried out up to a maximum strain of 2%. Due to the porosity of the material, see (Kallien and Busse, 2009), only a maximum strain of $\varepsilon_{\text{max}} = 1\%$ could be acquired before fracture starts to occur. Hence, we restrict our investigation to the small deformation range. With a look at Figure 1, it is obvious that the material shows a pronounced viscous behavior in all kinds of tests. Furthermore, the initial slope in the stress-strain diagram is effected by the rate of the test as well.

2.1.2 Equilibrium State

Since – from the previous experiments – it is evident that the material is rate-dependent, information about its equilibrium state has to be gathered. For the investigation of the equilibrium state, a long time relaxation test is carried out to determine its relaxation time. In this test, the specimen is loaded up to a certain strain amplitude γ_{max}, where the strain is kept constant, see Figure 2(a). Accordingly, the stress relaxes over the time, see Figure 3(a). In this test, one can notice that after more than $40\,\text{h}$, the material has not yet completely relaxed and that the relaxation corresponds to more than 50% of the initial value of the shear stress. The same behavior can be observed in tension and compression tests, which are omitted for brevity. With this information at hand, a multi-step relaxation test is carried out in order to estimate the equilibrium stress state. To this end, the specimen is loaded step-wise. In every step, the specimen relaxes towards the equilibrium stress state, see Figure 2(b). Due to the magnitude of the relaxation time, the holding time of the multistep relaxation process was chosen to $t_r = 6\,\text{h}$. For the estimation of the termination points, we assume that for the same relaxation time, the material relaxes for the same percentage. The estimated relaxation points in torsion are shown in Figure 3(b).

It can be observed that the initial slope in loading and unloading steps are different. This has to be considered in the modeling section as well.

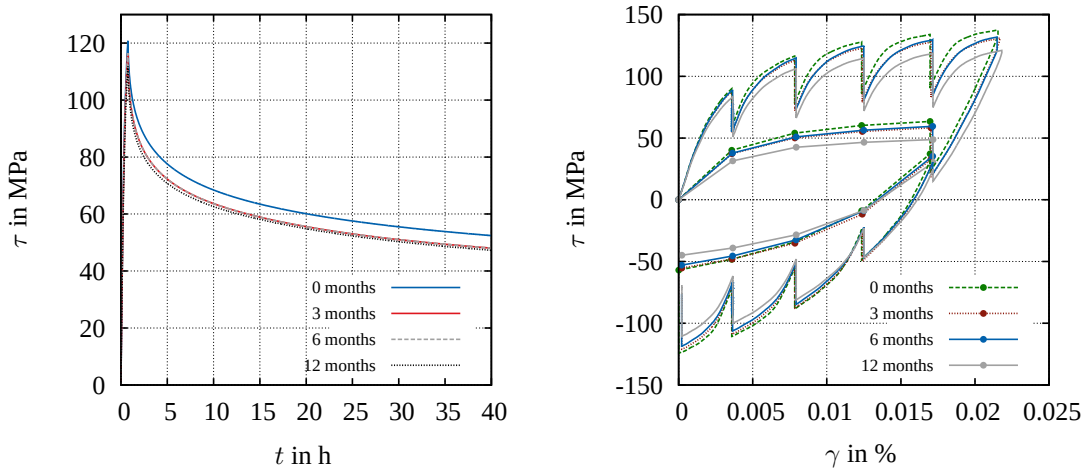

(a) Long time relaxation test in torsion (b) Multi-step relaxation test and equilibrium hysteresis torsion

Figure 3. Experiments for the investigation of the equilibrium state for different aging times in torsion

2.2 Influence of Aging

In order to consider the effect of aging in the mechanical response of the material, the long-time relaxation test and multi-step relaxation tests in torsion were carried out for three additional aging times at 3, 6 and 12 months, see Figure 3. The termination points of the relaxation have been calculated under the same assumption as in the previous section, see Figure 3(b). In these Figures, we can observe that the stresses decrease with longer aging times for the same strain process. The stress in the equilibrium hysteresis for 12 months aging is approximately 23% less than for the specimen without aging.

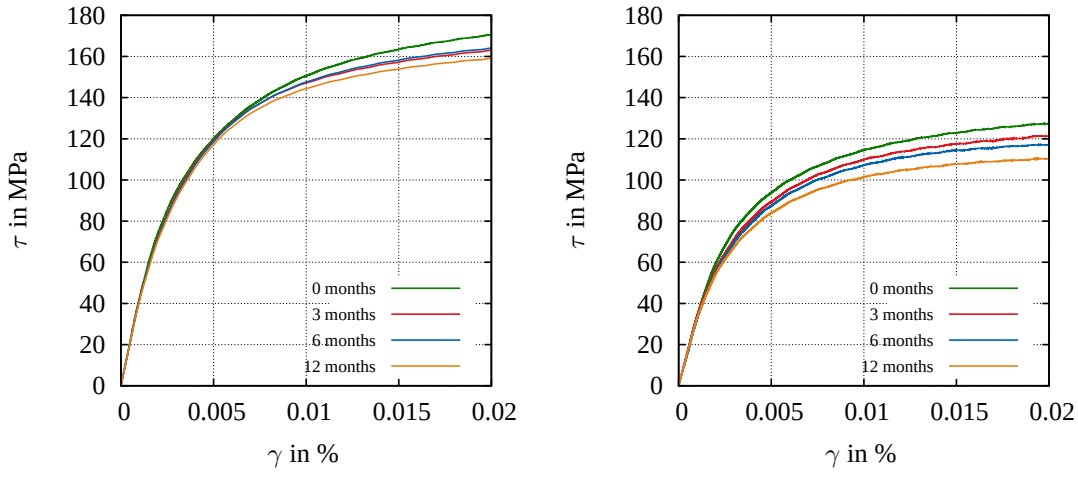

(a) $\dot{\gamma}_1 = 3.2 \times 10^{-4}\mathrm{s}^{-1}$ (b) $\dot{\gamma}_4 = 3.2 \times 10^{-7}\mathrm{s}^{-1}$

Figure 4. Rate-dependence for four aging times in torsion

The rate dependence was also investigated for aged specimens. In Figure 4, the results of the torsion tests are shown for the fastest and the slowest strain rates and four different aging times. Here, we again observe a reduction of the stresses in dependence of the age. An analogous behavior is observed in tension and compression, see Figure 9.

3 Constitutive Model

In the presented experiments, it is observed that the material shows a pronounced rate-dependence and possesses an equilibrium hysteresis. Based on this fact, the material can be placed in the material class of the viscoplasticity, see (Haupt and Lion, 1995) and (Haupt, 2000). In the literature there are several proposals describing viscoplasticity. The model presented in this article follows the modular structure suggested in works of (Haupt and Sedlan, 2001), (Haupt and Lion, 1995) or (Hartmann, 2006) and the references cited therein. This procedure shows advantages in the parameter identification process, offering the possibility to identify the parameters in a partitioned way.

The total strain is divided into a mechanical part $\mathbf{E}_{\mathrm{M}}$ and a component describing aging $\mathbf{E}_g$,

$$\mathbf{E} = \mathbf{E}_{\mathrm{M}} + \mathbf{E}_g. \tag{1}$$

The aging part of the strain $\mathbf{E}_g = -\alpha g \mathbf{I}$ defines the volumetric change in the material, which takes place during the aging process, see (Johnen, 1981; Leis and Kallien, 2011). The mechanical strain can be decomposed in an elastic and a viscous part

$$\mathbf{E}_{\mathrm{M}} = \mathbf{E}_{\mathrm{e}} + \mathbf{E}_{\mathrm{v}}. \tag{2}$$

The stress is decomposed into an equilibrium part $\mathbf{T}_{\mathrm{eq}}$ and an overstress part $\mathbf{T}_{\mathrm{ov}}$. Furthermore, the equilibrium stress consists of an elastic $\mathbf{T}^{\mathrm{e}}_{\mathrm{eq}}$ and a plastic (hysteretic) $\mathbf{T}^{\mathrm{h}}_{\mathrm{eq}}$ part,

$$\mathbf{T} = \mathbf{T}_{\mathrm{eq}} + \mathbf{T}_{\mathrm{ov}} = \mathbf{T}^{\mathrm{e}}_{\mathrm{eq}} + \mathbf{T}^{\mathrm{h}}_{\mathrm{eq}} + \mathbf{T}_{\mathrm{ov}}. \tag{3}$$

The rate-dependent effects are represented by a modified Maxwell model. To establish the thermodynamical consistence of the model, the dissipation inequality has to be evaluated. In the case of a constant temperature in time and space ($\dot{\Theta} = 0$ and $\operatorname{grad}\Theta = \vec{0}$), the Clausius-Duhem inequality can be expressed by

$$\frac{1}{\rho}\mathbf{T} \cdot \dot{\mathbf{E}} - \dot{\psi} \geq 0. \tag{4}$$

The free-energy ψ is assumed to depend on the strain variables and is divided into an equilibrium part ψ_{eq}, an overstress part ψ_{ov}, and an aging-dependent part ψ_g. Additionally, a process variable p is introduced to model the softening behavior which was observed in the experiments during the unloading process. $\mathbf{Y}$ is an internal strain-like variable. The dependence of the free energy on the internal variables is given by

$$\psi = \tilde{\psi}(\mathbf{E}_{\mathrm{M}}, \mathbf{E}_{\mathrm{e}}, \mathbf{Y}, p, g) = \psi^{\mathrm{e}}_{\mathrm{eq}}(\mathbf{E}_{\mathrm{M}}) + \psi^{\mathrm{h}}_{\mathrm{eq}}(\mathbf{Y}, p, g) + \psi_{\mathrm{ov}}(\mathbf{E}_{\mathrm{e}}, p) + \psi_g(g), \tag{5}$$

where we choose the following strain-energy functions

$$\rho\psi^{\mathrm{e}}_{\mathrm{eq}} = \frac{K_{\mathrm{eq}}}{2}(\operatorname{tr}\mathbf{E}_{\mathrm{M}})^2 + G_{\mathrm{eq}}\mathbf{E}^{\mathrm{D}}_{\mathrm{M}} \cdot \mathbf{E}^{\mathrm{D}}_{\mathrm{M}}, \tag{6}$$

$$\rho\psi^{\mathrm{h}}_{\mathrm{eq}} = \frac{c(p,g)}{2}\mathbf{Y}^{\mathrm{D}} \cdot \mathbf{Y}^{\mathrm{D}}, \tag{7}$$

$$\rho\psi_{\mathrm{ov}} = G_{\mathrm{ov}}(p)\mathbf{E}^{\mathrm{D}}_{\mathrm{e}} \cdot \mathbf{E}^{\mathrm{D}}_{\mathrm{e}}, \tag{8}$$

$$\rho\psi_g = C_1 - C_2 g. \tag{9}$$

K_{eq} and G_{eq} represent the bulk and shear modulus of the elastic part of the equilibrium stress. $c(p,g)$ controls the equilibrium hysteresis dependending on p and the age g. $G_{\mathrm{ov}}(p)$ symbolizes the process-dependent shear modulus of the overstresses. The time derivative of the free energy can be calculated by applying the chain rule

$$\dot{\psi} = \frac{\partial\psi}{\partial\mathbf{E}_{\mathrm{M}}} \cdot \dot{\mathbf{E}}_{\mathrm{M}} + \frac{\partial\psi}{\partial\mathbf{E}_{\mathrm{e}}} \cdot \dot{\mathbf{E}}_{\mathrm{e}} + \frac{\partial\psi}{\partial\mathbf{Y}} \cdot \dot{\mathbf{Y}} + \frac{\partial\psi}{\partial p}\dot{p} + \frac{\partial\psi}{\partial g}\dot{g}. \tag{10}$$

Inserting expression (10) and the stress decomposition (3) into the Clausius-Duhem inequality yields

$$(\mathbf{T}^{\mathrm{e}}_{\mathrm{eq}} + \mathbf{T}^{\mathrm{h}}_{\mathrm{eq}} + \mathbf{T}_{\mathrm{ov}}) \cdot \dot{\mathbf{E}} - \rho\frac{\partial\psi}{\partial\mathbf{E}_{\mathrm{M}}} \cdot \dot{\mathbf{E}}_{\mathrm{M}} - \rho\frac{\partial\psi}{\partial\mathbf{E}_{\mathrm{e}}} \cdot \dot{\mathbf{E}}_{\mathrm{e}} - \rho\frac{\partial\psi}{\partial\mathbf{Y}} \cdot \dot{\mathbf{Y}} - \rho\frac{\partial\psi}{\partial p}\dot{p} - \rho\frac{\partial\psi}{\partial g}\dot{g} \geq 0. \tag{11}$$

Rearranging the inequality and introducing the relations (1) and (2), leads to

$$\begin{aligned}\mathbf{T}^{\mathrm{e}}_{\mathrm{eq}} \cdot \dot{\mathbf{E}}_{\mathrm{M}} + \mathbf{T}^{\mathrm{e}}_{\mathrm{eq}} \cdot \dot{\mathbf{E}}_g + \mathbf{T}^{\mathrm{h}}_{\mathrm{eq}} \cdot \dot{\mathbf{E}} + \mathbf{T}_{\mathrm{ov}} \cdot (\dot{\mathbf{E}}_g + \dot{\mathbf{E}}_{\mathrm{e}} + \dot{\mathbf{E}}_{\mathrm{v}}) - \rho\frac{\partial\psi}{\partial\mathbf{E}_{\mathrm{M}}} \cdot \dot{\mathbf{E}}_{\mathrm{M}} \\ - \rho\frac{\partial\psi}{\partial\mathbf{Y}} \cdot \dot{\mathbf{Y}} - \rho\frac{\partial\psi}{\partial\mathbf{E}_{\mathrm{e}}} \cdot \dot{\mathbf{E}}_{\mathrm{e}} - \rho\frac{\partial\psi}{\partial p}\dot{p} - \rho\frac{\partial\psi}{\partial g}\dot{g} \geq 0.\end{aligned} \tag{12}$$

Now, we draw on the definition of the aging strain $\mathbf{E}_g = -\alpha g \mathbf{I}$, yielding –after reareanging–

$$\left(\mathbf{T}^{\mathrm{e}}_{\mathrm{eq}} - \rho\frac{\partial\psi}{\partial\mathbf{E}_{\mathrm{M}}}\right)\cdot\dot{\mathbf{E}}_{\mathrm{M}} - \alpha(\operatorname{tr}\mathbf{T}^{\mathrm{e}}_{\mathrm{eq}})\dot{g} + \mathbf{T}^{\mathrm{h}}_{\mathrm{eq}}\cdot\dot{\mathbf{E}} + \left(\mathbf{T}_{\mathrm{ov}} - \rho\frac{\partial\psi}{\partial\mathbf{E}_{\mathrm{e}}}\right)\cdot\dot{\mathbf{E}}_{\mathrm{e}} + \mathbf{T}_{\mathrm{ov}}\cdot\dot{\mathbf{E}}_g + \mathbf{T}_{\mathrm{ov}}\cdot\dot{\mathbf{E}}_{\mathrm{v}} - \rho\frac{\partial\psi}{\partial\mathbf{Y}}\cdot\dot{\mathbf{Y}} - \rho\frac{\partial\psi}{\partial p}\dot{p} - \rho\frac{\partial\psi}{\partial g}\dot{g} \geq 0. \quad (13)$$

This expression is used for emphasizing the following steps. Since the Clausius-Duhem inequality (13) has to be fulfilled, we can define the sufficient conditions

$$\mathbf{T}^{\mathrm{e}}_{\mathrm{eq}} = \rho\frac{\partial\psi}{\partial\mathbf{E}_{\mathrm{M}}} = K_{\mathrm{eq}}(\operatorname{tr}\mathbf{E}_{\mathrm{M}})\mathbf{I} + 2G_{\mathrm{eq}}\mathbf{E}^{\mathrm{D}}_{\mathrm{M}}, \quad (14)$$

$$\mathbf{T}_{\mathrm{ov}} = \rho\frac{\partial\psi}{\partial\mathbf{E}_{\mathrm{e}}} = 2G_{\mathrm{ov}}\mathbf{E}^{\mathrm{D}}_{\mathrm{ov}}. \quad (15)$$

Additionally, we assume

$$\mathbf{T}^{\mathrm{h}}_{\mathrm{eq}} = \rho\frac{\partial\psi}{\partial\mathbf{Y}} = c\mathbf{Y}^{\mathrm{D}}, \qquad \dot{\mathbf{Y}} = \dot{\mathbf{E}}^{\mathrm{D}} - \frac{b\dot{s}c + \dot{c}}{c}\mathbf{Y}^{\mathrm{D}}, \quad \text{with } b, c(p,g) > 0, \quad (16)$$

which reduces the remaining Clausius-Duhem inequality (13) to

$$c\mathbf{Y}^{\mathrm{D}}\cdot(\dot{\mathbf{E}} - \dot{\mathbf{Y}}) + \mathbf{T}_{\mathrm{ov}}\cdot\dot{\mathbf{E}}_{\mathrm{v}} - \rho\frac{\partial\psi}{\partial p}\dot{p} - 3\alpha K_{\mathrm{eq}}(\operatorname{tr}\mathbf{E}_{\mathrm{M}})\dot{g} - \rho\frac{\partial\psi}{\partial g}\dot{g} \geq 0, \quad (17)$$

with $\mathbf{T}_{\mathrm{ov}}\cdot\dot{\mathbf{E}}_g = 0$, because $\mathbf{T}_{\mathrm{ov}}$ is purely deviatoric and $\mathbf{E}_g$ volumetric. Again, we rearrange (17) by inserting (16) and obtain

$$c\mathbf{Y}^{\mathrm{D}}\cdot\left(\dot{\mathbf{E}} - \dot{\mathbf{E}}^{\mathrm{D}} + \frac{b\dot{s}c + \dot{c}}{c}\mathbf{Y}^{\mathrm{D}}\right) + \mathbf{T}_{\mathrm{ov}}\cdot\dot{\mathbf{E}}_{\mathrm{v}} - \rho\frac{\partial\psi}{\partial p}\dot{p} - 3\alpha K_{\mathrm{eq}}(\operatorname{tr}\mathbf{E}_{\mathrm{M}})\dot{g} - \rho\frac{\partial\psi}{\partial g}\dot{g} \geq 0. \quad (18)$$

The term $c\mathbf{Y}^{\mathrm{D}}\cdot\left(\dot{\mathbf{E}} - \dot{\mathbf{E}}^{\mathrm{D}}\right)$ is equal to zero, since $\dot{\mathbf{E}} - \dot{\mathbf{E}}^{\mathrm{D}} = (\operatorname{tr}\dot{\mathbf{E}})/3\mathbf{I}$ is volumetric and $\mathbf{Y}^{\mathrm{D}}$ is purely deviatoric,

$$b\dot{s}c\mathbf{Y}^{\mathrm{D}}\cdot\mathbf{Y}^{\mathrm{D}} + \dot{c}\mathbf{Y}^{\mathrm{D}}\cdot\mathbf{Y}^{\mathrm{D}} + \mathbf{T}_{\mathrm{ov}}\cdot\dot{\mathbf{E}}_{\mathrm{v}} - \rho\frac{\partial\psi}{\partial p}\dot{p} - 3\alpha K_{\mathrm{eq}}(\operatorname{tr}\mathbf{E}_{\mathrm{M}})\dot{g} - \rho\frac{\partial\psi}{\partial g}\dot{g} \geq 0. \quad (19)$$

The time derivative of the parameter $c(p,g)$ can be expressed by $\dot{c} = (\partial c/\partial p)\dot{p} + (\partial c/\partial g)\dot{g}$ yielding

$$b\dot{s}c\mathbf{Y}^{\mathrm{D}}\cdot\mathbf{Y}^{\mathrm{D}} + \left(\frac{\partial c}{\partial p}\dot{p} + \frac{\partial c}{\partial g}\dot{g}\right)\mathbf{Y}^{\mathrm{D}}\cdot\mathbf{Y}^{\mathrm{D}} + \mathbf{T}_{\mathrm{ov}}\cdot\dot{\mathbf{E}}_{\mathrm{v}} - \rho\frac{\partial\psi}{\partial p}\dot{p} - 3\alpha K_{\mathrm{eq}}(\operatorname{tr}\mathbf{E}_{\mathrm{M}})\dot{g} - \rho\frac{\partial\psi}{\partial g}\dot{g} \geq 0. \quad (20)$$

With the expression of the free energy (9), we obtain

$$\rho\frac{\partial\psi}{\partial p} = \frac{1}{2}\frac{\partial c}{\partial p}\mathbf{Y}^{\mathrm{D}}\cdot\mathbf{Y}^{\mathrm{D}} \quad \text{and} \quad \rho\frac{\partial\psi}{\partial g} = \frac{1}{2}\frac{\partial c}{\partial g}\mathbf{Y}^{\mathrm{D}}\cdot\mathbf{Y}^{\mathrm{D}} - C_2 \quad (21)$$

leading to

$$\left(b\dot{s}c + \frac{1}{2}\frac{\partial c}{\partial p}\dot{p}\right)\mathbf{Y}^{\mathrm{D}}\cdot\mathbf{Y}^{\mathrm{D}} + \left(C_2 + \frac{1}{2}\frac{\partial c}{\partial g}\mathbf{Y}^{\mathrm{D}}\cdot\mathbf{Y}^{\mathrm{D}} - 3\alpha K_{\mathrm{eq}}(\operatorname{tr}\mathbf{E}_{\mathrm{M}})\right)\dot{g} + \mathbf{T}_{\mathrm{ov}}\cdot\dot{\mathbf{E}}_{\mathrm{v}} \geq 0. \quad (22)$$

The sum of these three terms has to be non-negative. If every term is positive, this condition is satisfied. For the term of the overstress, we define

$$\dot{\mathbf{E}}_{\mathrm{v}} = \frac{1}{\eta}\mathbf{T}_{\mathrm{ov}}, \qquad \eta > 0. \quad (23)$$

We define the aging rate proportional to

$$\dot{g} = f(g)\left(C_2 + \frac{1}{2}\frac{\partial c}{\partial g}\mathbf{Y}^{\mathrm{D}}\cdot\mathbf{Y}^{\mathrm{D}} - 3\alpha K_{\mathrm{eq}}(\operatorname{tr}\mathbf{E}_{\mathrm{M}})\right), \qquad f(g) \geq 0. \quad (24)$$

The aging rate $\dot{g}$ is coupled with the plastic deviatoric strain $\mathbf{Y}$ and the trace of the mechanical strain $\operatorname{tr}\mathbf{E}_{\mathrm{M}}$. Due to the fact that $\partial c/\partial g < 0$, a plastic deformation implies a reduction in the aging rate $\dot{g}$. The influence of the term $\operatorname{tr}\mathbf{E}_{\mathrm{M}}$ depends on its sign. The magnitude of this coupling is characterized by the parameter C_2. Since a negative

aging rate is physically not realistic, the positive parameter C_2 has to be larger than the term influenced by the strain, see the discussion in the field of curing by Lion et al. (2014). In this way, the strain can just decelerate the aging process, but not revert it. We define the function $f(g) = \alpha_g(1-g)/(C_2(\beta_g+g))$ and arrive at

$$\dot{g} = \frac{\alpha_g}{C_2}\frac{1-g}{\beta_g+g}\left(C_2 + \frac{1}{2(1+p)}\frac{\partial c_0}{\partial g}\mathbf{Y}^{\mathrm{D}}\cdot\mathbf{Y}^{\mathrm{D}} - 3\alpha K_{\mathrm{eq}}\mathrm{tr}\left(\mathbf{E}_{\mathrm{M}}\right)\right). \tag{25}$$

The aging variable g is a growing variable with values between 0 and 1. The parameter $c(p,g)$ represents the initial slope of the equilibrium stress, which is monotonically decreasing with the aging state. In terms of the plastic strain, the derivative $\partial c/\partial p$ is also negative, due to the fact that there is a reduction in the initial slope due to softening. This makes it slightly more complicated, in the context of Clausius-Duhem inequality, to be proven. We define

$$\dot{s} = \sqrt{\dot{\mathbf{E}}_{\mathrm{M}}\cdot\dot{\mathbf{E}}_{\mathrm{M}}} \geq 0, \tag{26}$$

$$\dot{p} = \alpha_p(1-p)\dot{s}, \tag{27}$$

$$c(p,g) = \frac{c_0(g)}{1+p}, \qquad c_0(g) = c_1(1-c_2\exp(c_3 g)). \tag{28}$$

The limit values of $c(p,g)$ are

$$\lim_{p\to 0} c = c_0(g), \qquad \lim_{p\to 1} c = \frac{c_0(g)}{2} \tag{29}$$

$$\lim_{g\to 0} c_0 = c_1(1-c_2), \quad \lim_{g\to 1} c_0 = c_1(1-c_2\exp(c_3)). \tag{30}$$

The partial derivative of $c(p,g)$ with respect to p is according to equation (27)

$$\frac{\partial c}{\partial p} = -\frac{c_0}{(1+p)^2}. \tag{31}$$

Due to the fact that $\mathbf{Y}^{\mathrm{D}}\cdot\mathbf{Y}^{\mathrm{D}} \geq 0$, we have to prove that

$$\beta b\dot{s}c + \frac{1}{2}\frac{\partial c}{\partial p}\dot{p} \geq 0. \tag{32}$$

Inserting definitions (27), (28), and (31) in equation (32), we obtain

$$b\dot{s}\frac{c_0}{1+p} - \frac{1}{2}\frac{c_0}{(1+p)^2}\alpha_p(1-p)\dot{s} \geq 0 \tag{33}$$

$$2b - \frac{1-p}{1+p}\alpha_p \geq 0 \tag{34}$$

The function p is a monotonically increasing function with values between 0 and 1, see equation (27). Thus, the inequality is fulfilled for these two cases, it will be fulfilled in the whole range of values of p.

$$\text{for } p = 0 \rightarrow b \geq \frac{\alpha_p}{2} \tag{35}$$

$$\text{for } p = 1 \rightarrow b \geq 0 \rightarrow \quad \text{It is fulfilled} \tag{36}$$

If condition (35) is fulfilled, the Clausius-Duhem inequality is satisfied and the constitutive model is thermodynamically consistent. In the material parameter identification process, the fulfillment of condition (35) has to be ensured. Furthermore, we define the shear modulus G_{ov} and the viscosity η by

$$G_{\mathrm{ov}}(p) = G_1(1-p)^{r_{\mathrm{ov}}} + G_2, \tag{37}$$

$$\eta(\dot{\mathbf{E}}_{\mathrm{M}}) = \eta_0\left(\left(\frac{||\dot{\mathbf{E}}_{\mathrm{M}})||}{s_\eta} + \alpha_\eta\right)^{-r_\eta} + 1\right). \tag{38}$$

Their limit values are

$$\lim_{p\to 0} G_{\mathrm{ov}} = G_1 + G_2, \qquad \lim_{p\to 1} G_{\mathrm{ov}} = G_2, \tag{39}$$

$$\lim_{\dot{s}\to 0} \eta = \eta_0\left(\alpha_\eta^{-r_\eta} + 1\right), \quad \lim_{\dot{s}\to\infty} \eta = \eta_0. \tag{40}$$

Table 1 summarizes the entire model.

Table 1. Summary of the constitutive model

Constitutive Model
$\mathbf{E} = \mathbf{E}_{\mathrm{M}} + \mathbf{E}_g$ $\mathbf{E}_g = -\alpha g \mathbf{I}$ $\mathbf{E}_{\mathrm{M}} = \mathbf{E}_{\mathrm{e}} + \mathbf{E}_{\mathrm{v}}$ $\mathbf{T} = \mathbf{T}^{\mathrm{e}}_{\mathrm{eq}} + \mathbf{T}^{\mathrm{h}}_{\mathrm{eq}} + \mathbf{T}_{\mathrm{ov}}$
$\dot{p} = \alpha_p (1-p)\dot{s}, \quad \dot{s} = \sqrt{\dot{\mathbf{E}}_{\mathrm{M}} \cdot \dot{\mathbf{E}}_{\mathrm{M}}} = \lvert\lvert \dot{\mathbf{E}}_{\mathrm{M}} \rvert\rvert$ $\dot{g} = \dfrac{\alpha_g}{C_2} \dfrac{1-g}{\beta_g + g} \left(C_2 + \dfrac{1}{2(1+p)} \dfrac{\partial c_0}{\partial g} \mathbf{Y}^{\mathrm{D}} \cdot \mathbf{Y}^{\mathrm{D}} - 3\alpha K_{\mathrm{eq}} (\operatorname{tr} \mathbf{E}_{\mathrm{M}}) \right)$
Equilibrium stress part
$\mathbf{T}^{\mathrm{e}}_{\mathrm{eq}} = K_{\mathrm{eq}} (\operatorname{tr} \mathbf{E}_{\mathrm{M}}) \mathbf{I} + 2 G_{\mathrm{eq}} \mathbf{E}^{\mathrm{D}}_{\mathrm{M}}$ $\mathbf{T}^{\mathrm{h}}_{\mathrm{eq}} = c \mathbf{Y}^{\mathrm{D}}$ $\dot{\mathbf{Y}} = \dot{\mathbf{E}}^{\mathrm{D}} - \left(b\dot{s} + \dfrac{\dot{c}}{c} \right) \mathbf{Y}^{\mathrm{D}}$
Overstress part
$\mathbf{T}_{\mathrm{ov}} = 2 G_{\mathrm{ov}}(p) \mathbf{E}^{\mathrm{D}}_{\mathrm{e}}$ $\dot{\mathbf{E}}_{\mathrm{v}} = \dfrac{1}{\eta} \mathbf{T}_{\mathrm{ov}}$
Softening and aging dependent functions
$c(p,g) = \dfrac{c_0(g)}{p+1}, \quad c_0(g) = c_1 (1 - c_2 \exp(c_3 g))$ $G_{\mathrm{ov}}(p) = G_1 (1-p)^{r_{\mathrm{ov}}} + G_2$ $\eta(\dot{\mathbf{E}}_{\mathrm{M}}) = \eta_0 \left(\left(\dfrac{\lvert\lvert \dot{\mathbf{E}}_{\mathrm{M}} \rvert\rvert}{s_\eta} + \alpha_\eta \right)^{-r_\eta} + 1 \right)$
Parameters
$\alpha, \alpha_p, \alpha_g, C_2, \beta_g, \quad K_{\mathrm{eq}}, G_{\mathrm{eq}}, b, c_1, c_2, c_3, \quad G_1, G_2, r_{\mathrm{ov}}, \eta_0, s_\eta, \alpha_\eta, r_\eta$

4 Parameter Identification

The constitutive model in Table 1 contains 18 material parameters, which have to be determined. Since the identification problem is an ill-posed problem, all material parameters cannot be identified simultaneously. In order to solve this problem, we try to isolate particular phenomena, such as deviatoric behavior, rate-dependence or aging, choosing experiments where the influence of other effects can be neglected.

In the parameter identification procedure, the square of the residuum $\mathbf{r}(\boldsymbol{\kappa}) = \mathbf{s}(\boldsymbol{\kappa}) - \mathbf{d}$ has to be minimized. The vector $\mathbf{s} \in \mathbb{R}^{n_d}$ represents the (model) simulation and $\mathbf{d} \in \mathbb{R}^{n_d}$ the experimental data,

$$f(\boldsymbol{\kappa}) = \mathbf{r}^T(\boldsymbol{\kappa}) \mathbf{r}(\boldsymbol{\kappa}) \rightarrow \text{minimum}. \tag{41}$$

The material parameters are assembled in a vector $\boldsymbol{\kappa} \in \mathbb{R}^{n_\kappa}$ with n_κ material parameters. Additionally, there are n_c inequality constraints $g_i(\boldsymbol{\kappa}) \leq 0$, which have to be fulfilled for theoretical reasones, see equation (35), physical reasons (positiveness of parameters) or to restrict their co-domain in a certain range. In the following subsections, $\mathbf{s}$ can be an analytical model or the result of the numerical (or analytical) solution of an ordinary differential equation or of an entire boundary-value problem using finite elements. For the non-linear optimization methods, the identification is carried out with the help of Matlab routines, which can either draw on solutions provided by Matlab itself, or they call up external programs that serve to compute a solution. Here, we refer to (Krämer et al., 2015). The identification process is connected to the model structure and cannot be seen separately. This means, some of the developed constitutive equations are chosen after some steps of identification.

4.1 Aging Variable

For the identification of the aging variable, we consider the measurement in (Johnen, 1981), where the shrinkage of a zamak 5 specimen is measured over the time. In (Kallien and Busse, 2009), the principal physical microstructural changes during aging are described. The dimensional change is associated with change of the crystallization system from fcc (face-centered cubic) to hcp (hexagonal close-packed) and also changes in the lattice parameter. This deformation is a purely volumetric deformation associated to aging and is denoted in the model as $\mathbf{E}_g$. We normalize the volumetric deformation from Johnen (1981), $g = \varepsilon_{\text{measured}}/\varepsilon_{\text{max}}$, and take it as aging reference, see dots in Figure 5(a). During this measurement, no mechanical deformation happens. Thus, we can set the deviatoric plastic strain $\mathbf{Y} = \mathbf{0}$ and $\operatorname{tr} \mathbf{E}_{\text{M}} = 0$. In this case, there are only two material parameters in the evolution equation (25) of the aging variable, which have to be identified, α_g and β_g, i.e.

$$\dot{g} = \alpha_g \frac{1-g}{\beta_g + g}. \tag{42}$$

Using this ordinary differential equation, we have at the initial time for $g(0) = 0$ the condition $\dot{g}(0) = \alpha_g/\beta_g$. At the final time $\dot{g}(\infty) = 0$ yields $g(\infty) = 1$ from equation (42). The derivative of the experimental points $\dot{g}$ is calculated with forward differences, see points in Figure 5(b). The identification is carried out using a gradient based algorithm (trust-region). The identified parameters are $\alpha_g = 3.67 \times 10^{-8}\,\text{s}^{-1}$ and $\beta_g = 0.2$. The small value of the parameter α_g indicates that the aging process happens very slowly. The fitted function is shown in Figure 5. Moreover, for the volumetric aging strain $\mathbf{E}_g = -\alpha g \mathbf{I}$, the parameter $\alpha = 10^{-3}$ is identified from the

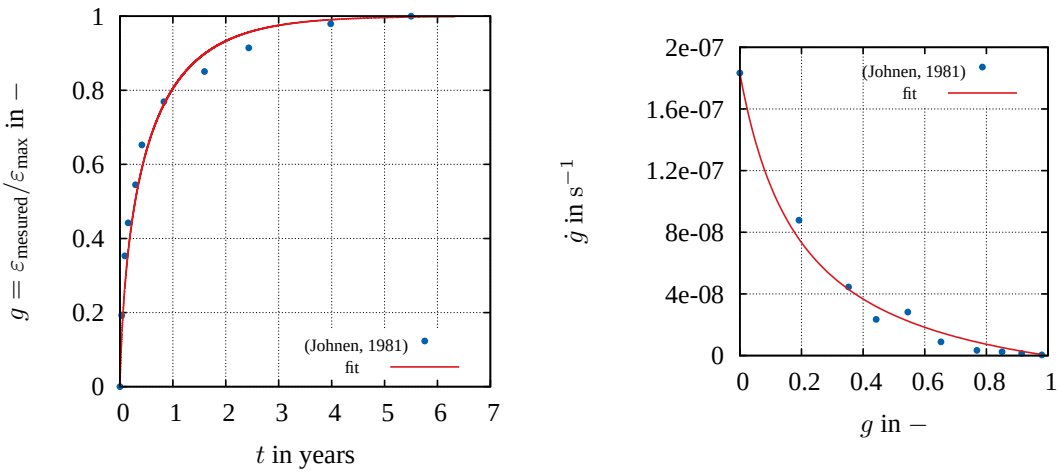

(a) Aging variable over time

(b) Rate of the aging over aging $\dot{g} = f(g)$

Figure 5. Results of the identification for the aging variable

value of the strain for 5.5 years aging ($g \approx 1$) from the measurement of Johnen (1981).

The coupling between the aging variable and the plastic deformation represents a change in the aging rate $\dot{g}$ with the deformation, see equation (25). Due to the fact that the duration of the experiments is relatively short compared to the time that aging variable needs to develop, it is impossible to obtain information about this coupling from the performed experiments. In the actual model, we assume a very low influence of this term in the aging. We assume the parameter C_2 to be much larger that the term of the strain, see equation (24), so that the aging rate $\dot{g}$ is marginally affected by this term. Thus, we assign the value $C_2 = 10^6\,\text{MPa}^{-1}$. In this way, we ensure that equation (25) is approximately equal to equation (42). Expression (42) is taken at this point as the evolution equation for the aging variable.

4.2 Shear Behavior

In this step of the identification, the evolution of the aging variable is known. The forthcoming identification step in torsion is drawn on the partitioned structure of the model. We first identify the parameters of the equilibrium

stress with the help of the experimental data points of the equilibrium hysteresis for the different aging states. Subsequently, the remaining parameters of the deviatoric part of the model are identified with experiments at different strain rates and the relaxation steps. The aging variable g develops clearly slower than the deformation process of all the experiments. Because of that, we assume, for the identification steps, a constant aging state, that means, no development of the aging variable occurs during the loading or relaxation experiment.

Equilibrium Part

In case of torsion with a constant, infinitely slow strain rate, $\dot{\gamma} = K \ll 1$, the shear stress of the equilibrium part is calculated as

$$\tau_{\text{eq}} = \tau_{\text{eq}}^{\text{e}} + \tau_{\text{eq}}^{\text{h}} = G_{\text{eq}} K t + \tau_{\text{eq}}^{\text{h}}. \tag{43}$$

To obtain the hysteretic equilirbium stress, the following system of differential equations has to be solved

$$\dot{p} = \alpha_p (1-p) \frac{|K|}{\sqrt{2}}, \tag{44}$$

$$\dot{\tau}_{\text{eq}}^{\text{h}} = c(p,g) \frac{K}{2} - b \frac{|K|}{\sqrt{2}} \tau_{\text{eq}}^{\text{h}}, \quad \text{with} \quad c = \frac{c_0(g)}{1+p}. \tag{45}$$

The identification is carried out with Matlab with the help of the nonlinear least-squares solver *lsqnonlin*, using the data of the equilibrium hysteresis at different aging times. First, the parameter c_0 is identified independently for every aging time. After that, a function $c(g)$ is fitted for obtaining c_0, see Figure 6(a). The results of the identification are shown in Table 2 and Figure 7 (equilibrium hysteresis). We observe a very good calibration between simulation and experiment for the equilibrium hysteresis.

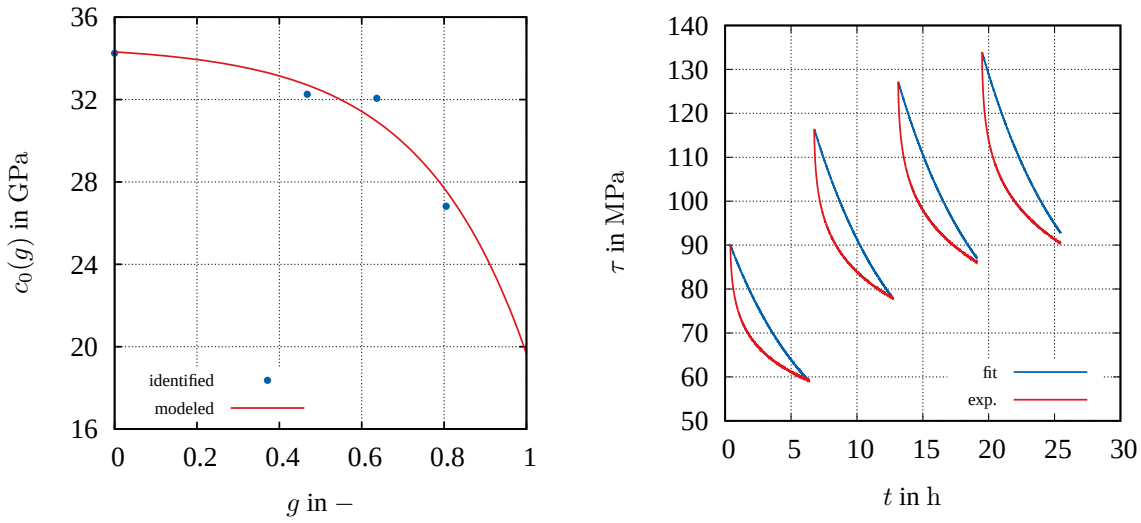

(a) Aging dependent function $c_0(g)$

(b) Relaxation steps of the multi-step relaxation test

Figure 6. Identified values during identification and fitted functions

Table 2. Results of the parameter identification for the parameter of the equilibrium part

parameter	α_p	b	c_1	c_2	c_3
value	300	1.876×10^2 GPa	3.463×10^4 GPa	9.166×10^{-3}	3.854

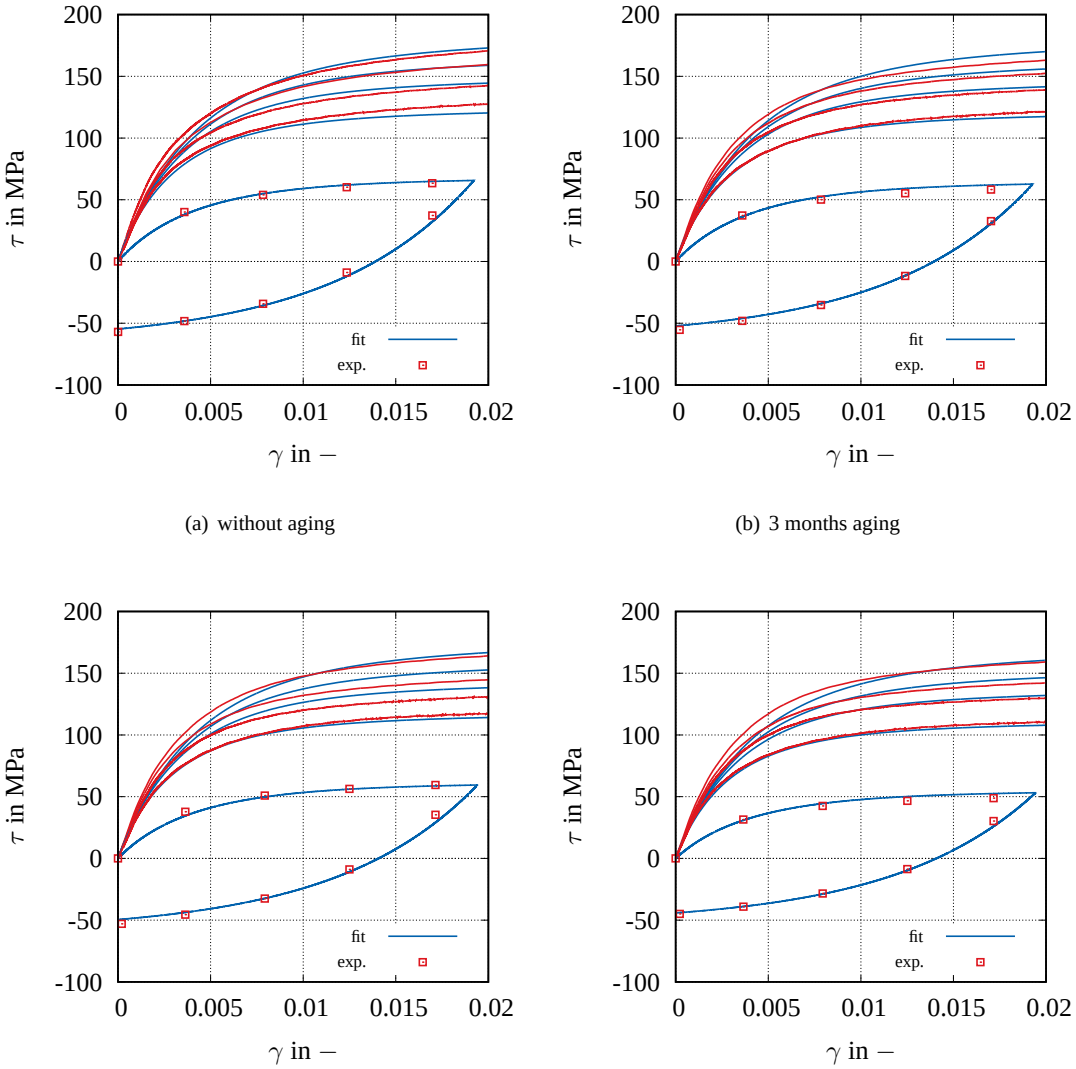

(a) without aging

(b) 3 months aging

(c) 6 months aging

(d) 12 months aging

Figure 7. Results of the identification in torsion

Overstress Part

For the identification of the overstress part, we take the relaxation steps of the multi-step relaxation tests into account in a first step, and afterwards, the experiments at different strain rates are considered. In the model, the effect of aging is only considered in the equilibrium stress part. Thus, the overstress parameters are identified with the help of the experiments without aging. The total shear stress is equal to the equilibrium plus the overstress part

$$\tau = \tau_{\text{eq}} + \tau_{\text{ov}}. \tag{46}$$

The equilibrium part is already known from the previous section. The shear overstress is calculated from

$$\tau_{\text{ov}} = G_{\text{ov}}(p)\,(\gamma - \gamma_{\text{v}})\,, \tag{47}$$

with the viscous shear strain γ_{v} from equation (23)

$$\dot{\gamma}_{\text{v}} = \frac{2G_{\text{ov}}(p)}{\eta(\dot{\gamma})}\,(\gamma - \gamma_{\text{v}})\,. \tag{48}$$

Relaxation In the isothermal relaxation process, the strain is constant, $\gamma = \hat{\gamma} = \text{const.}$, and, thus, the strain-rate is equal to zero, $\dot{\gamma} = 0$. Thus, the rate of the arc-length is zero as well, $\dot{s} = 0$. Accordingly, the rate of the softening

variable is zero as well $\dot{p} = 0 \rightarrow p = \hat{p} =$const, see equation (27). For a relaxation process, the shear modulus G_{ov} and the viscosity η are constant, see equations (37) and (38),

$$\hat{\eta} = \eta_0 \left(\alpha_\eta^{-r_\eta} + 1\right) = \text{const.}, \tag{49}$$

$$\hat{G}_{\text{ov}}(\hat{p}) = G_1(1-\hat{p})^{n_{\text{ov}}} + G_2 = \text{const.} \tag{50}$$

Inserting equations (49) and (50) in equation (48) leads to

$$\dot{\gamma}_{\text{v}} + \frac{2\hat{G}_{\text{ov}}}{\hat{\eta}}\gamma_{\text{v}} = \frac{2\hat{G}_{\text{ov}}}{\hat{\eta}}\hat{\gamma}. \tag{51}$$

This differential equation can be solved analytically and results in

$$\gamma_{\text{v}}(t) = (\gamma_{\text{v}}(0) - \hat{\gamma}) \exp\left(\frac{-2\hat{G}_{\text{ov}}}{\hat{\eta}}t\right) + \hat{\gamma}. \tag{52}$$

With this solution of the viscous shear strain at hand, the overstress can be calculated by equation (47). The ratio

$$\frac{\hat{G}_{\text{ov}k}}{\hat{\eta}_k} = \frac{G_1(1-\hat{p})^{n_{\text{ov}}} + G_2}{\eta_0\left(\alpha_\eta^{-r_\eta} + 1\right)} \tag{53}$$

is identified for every relaxation step. This information is used in the identification step with the monotonic loading paths. The results of the identification of the relaxation steps are shown in Figure 6(b).

Monotonic loading In a monotonic loading process, the strain rate is constant, $\dot{\gamma} = K$, and the shear strain is equal to $\gamma\,(t) = Kt$. The overstress has, in this case, the following form

$$\tau_{\text{ov}} = G_{\text{ov}}(p)\,(\gamma - \gamma_{\text{v}})\,, \tag{54}$$

$$\dot{\gamma}_{\text{v}} + \frac{2G_{\text{ov}}(p)}{\eta(K)}\gamma_{\text{v}} = \frac{2G_{\text{ov}}(p)}{\eta(K)}Kt. \tag{55}$$

Since equation (55) cannot be solved analytically, it is solved numerically in Matlab. In the next step, we have to model and identify the parameters for the shear modulus of the overstress, G_1, G_2, and r_{ov} and for the viscosity, η_0, α_η, and r_η. From the identification step of relaxation, we have four additional relations, see equation (53). The set of parameters of the shear modulus G_{ov} in equation (37) and for the viscosity η of equation (38) are compiled in Table 3. The parameter s_η in equation (38) is of the dimension of the rate of the arc-length $\dot{s}$ and is set equal to

Table 3. Results of the parameter identification for the shear modulus G_{ov} and the viscosity η

parameter	G_1	G_2	r_{ov}	η_0	α_η	r_η
value	$10\,\text{GPa}$	$15\,\text{GPa}$	0.3	$300\,\text{MPa s}$	8×10^{-8}	0.93

$s_\eta = 1\text{s}^{-1}$ to obtain a dimensionless expression. The solution of the identification is shown in Figure 7. Here, we observe again a good reproducibility of the experimental behavior and in this way, the assumption that aging only influences the equilibrium state is justified. Moreover, in Figure 8 the effect of the aging variable in the model is shown. The torsion experiments and the model are compared for two different strain rates and different ages. Here, we observe the reduction in the stresses caused by the aging stage. This is a prediction from the model, since the experiments at different strain rates were not used for the identification process.

4.3 Volumetric Behavior

The last parameter to be identified is the compression modulus K_{eq}. In the case of tension and compression, it is necessary to consider the complete three-dimensional model of Table 1. With the same procedure as (Krämer et al., 2015), the three-dimensional model is reduced to the one-dimensional case for parameter identification. The parameter K_{eq} is identified with the help of the equilibrium hysteresis in tension and compression for the unaged material. From the identification, we obtain a value $K_{\text{eq}} = 49.5\,\text{GPa}$. The results of the identification

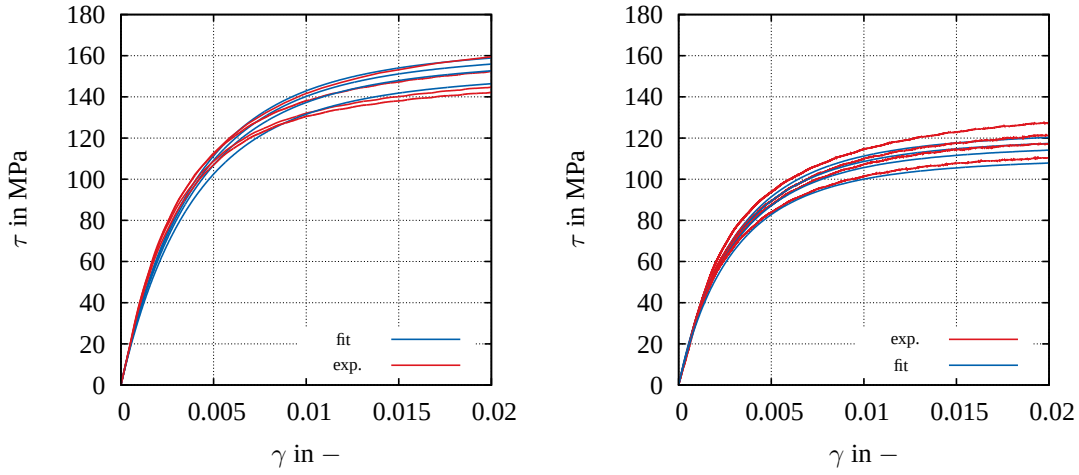

(a) Experiments in torsion at the strain rate $\dot{\gamma}_2 = 3.2 \times 10^{-2}\mathrm{s}^{-1}$

(b) Experiments in torsion at the strain rate $\dot{\gamma}_4 = 3.2 \times 10^{-4}\mathrm{s}^{-1}$

Figure 8. Results of the identification in torsion. Comparison in torsion for different aging times.

for the equilibrium hysteresis and the prediction of the rate dependence (these experiments were not used for the identification) are shown in Figure 9 for the different aging times.

We observe that the information contained in the deviatoric part of the model (in this case, obtained from torsion experiments) is almost sufficient to calibrate this material. The tension and compression tests are only necessary to identify the compression modulus to obtain an appropriate reproducibility of the experiments in tension and compression, see Figure 9.

5 Stress Computation and Numerical Example

To implement the model into a finite element program, we make use of the symmetry properties of the stress tensor $\mathbf{T}$ and strain tensor $\mathbf{E}$. They are expressed as a vector (Voigt notation) with the following components

$$\mathsf{E}(\mathsf{X}, t) = \{E_{11}, E_{22}, E_{33}, 2E_{12}, 2E_{13}, 2E_{23}\}^T, \tag{56}$$

$$\mathsf{T}(\mathsf{X}, t) = \{T_{11}, T_{22}, T_{33}, T_{12}, T_{13}, T_{23}\}^T. \tag{57}$$

The constitutive model is formulated depending on the mechanical strain. The scalar product reads in matrix notation

$$\mathbf{A} \cdot \mathbf{A} = \mathsf{A}^T \mathsf{M}^{-1} \mathsf{A} \quad \text{with} \quad \mathsf{M} = \mathrm{diag}(1,1,1,2,2,2), \quad \mathsf{A} \in \mathbb{R}^6. \tag{58}$$

The deviator operator of a tensor $\mathbf{A}^{\mathrm{D}}$ is given by the matrix formulation

$$\mathsf{A}^{\mathrm{D}} = \mathsf{D}\mathsf{A} \quad \text{with} \quad \mathsf{D} = \frac{1}{3}\begin{bmatrix} 2 & -1 & -1 & & & \\ -1 & 2 & -1 & & & \\ -1 & -1 & 2 & & & \\ & & & 3 & & \\ & & & & 3 & \\ & & & & & 3 \end{bmatrix} \tag{59}$$

The first necessary variable for the stress computation is the time derivative of the arc-lenth $\dot{s}_{\mathrm{M}}$. Using a Backward-Euler step, we obtain

$$s_{\mathrm{M}n+1} = s_{\mathrm{M}n} + \dot{s}_{\mathrm{M}} \Delta t_n = s_{\mathrm{M}n} + \Delta s_{\mathrm{M}n} \tag{60}$$

with

$$\Delta s_{\mathrm{M}n} = \dot{s}_{\mathrm{M}} \Delta t_n = \sqrt{(\mathsf{E}_{\mathrm{M}n+1} - \mathsf{E}_{\mathrm{M}n})^T \mathsf{M}^{-1} (\mathsf{E}_{\mathrm{M}n+1} - \mathsf{E}_{\mathrm{M}n})} = \sqrt{\Delta \mathsf{E}_{\mathrm{M}n}{}^T \mathsf{M}^{-1} \Delta \mathsf{E}_{\mathrm{M}n}}. \tag{61}$$

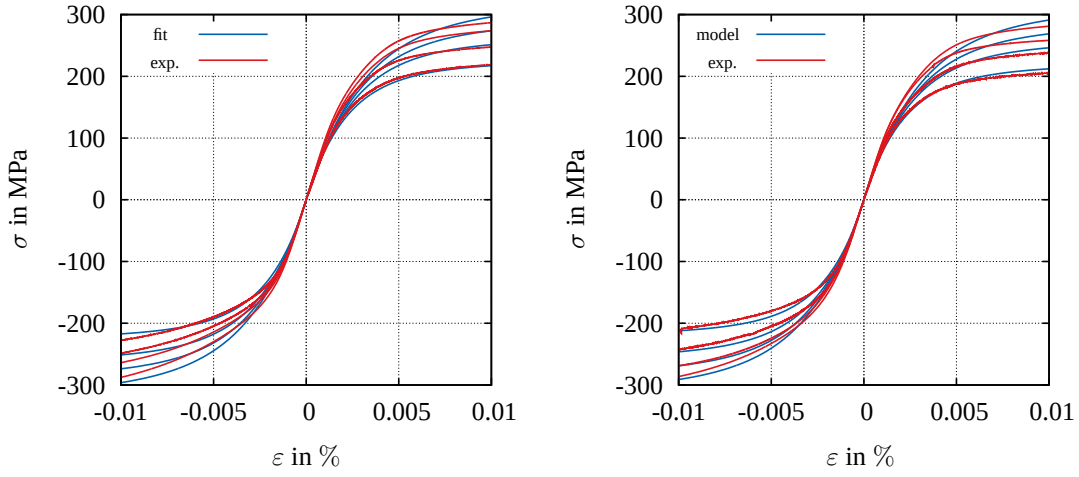

(a) without aging

(b) 3 months aging

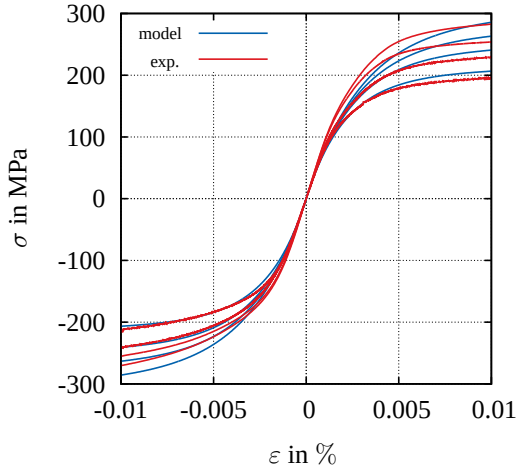

(c) 6 months aging

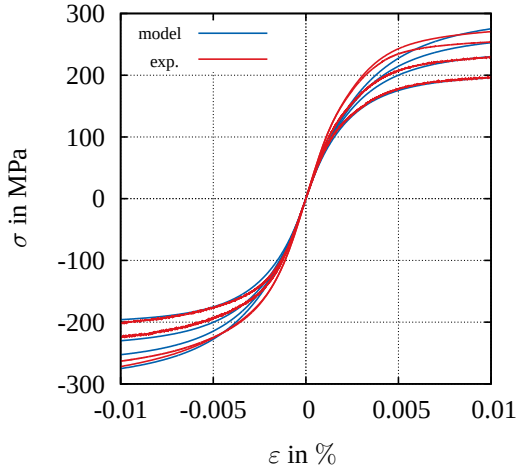

(d) 12 months aging

Figure 9. Identification and prediction in tension/compression

In the model, there are 14 internal variables: the aging variable g, the softening variable p, and six components for the plastic stress $\mathbf{T}^{\mathrm{h}}_{\mathrm{eq}}$ and the viscous strain $\mathbf{E}_{\mathrm{v}}$ respectively. The parameter C_2 was chosen in a way, that the evolution equation for g is approximately equal to equation (42). Since the term due to the deformation has a minor influence in the aging rate, we neglect the coupling term of aging with deformation, in order to facilitate the implementation of the model. The evolution equation of the internal variables can be discretized in time again by using a Backward-Euler step

$$g_{n+1} = g_n + \Delta t_n \alpha_g \frac{1 - g_{n+1}}{\beta_g + g_{n+1}}, \tag{62}$$

$$p_{n+1} = p_n + \Delta t_n \left(\alpha_p (1 - p_{n+1}) \frac{\Delta s_{\mathrm{M}n}}{\Delta t_n} \right), \tag{63}$$

$$\mathbf{T}^{\mathrm{h}}_{n+1} = \mathbf{T}^{\mathrm{h}}_{n} + \Delta t_n \left(c(p_{n+1}, g_{n+1}) \mathbf{D} \left(\frac{\Delta \mathbf{E}_{\mathrm{M}n}}{\Delta t_n} \right) - b \frac{\Delta s_{\mathrm{M}n}}{\Delta t_n} \mathbf{T}^{\mathrm{h}}_{n+1} \right), \tag{64}$$

$$\mathbf{E}_{\mathrm{v}n+1} = \mathbf{E}_{\mathrm{v}n} + \frac{\Delta t_n}{\eta(\mathbf{E}_{\mathrm{M}n+1})} \left(2 G_{\mathrm{ov}}(p_{n+1}) \mathbf{D} \left(\mathbf{E}_{\mathrm{M}n+1} - \mathbf{E}_{\mathrm{v}n+1} \right) \right), \tag{65}$$

which can analytically be solved to obtain

$$g_{n+1} = \frac{1}{2}(g_n - \beta_g - \Delta t_n \alpha_g) + \sqrt{\frac{1}{4}(\beta_g + \Delta t_n \alpha_g - g_n)^2 + \beta_g g_n + \Delta t_n \alpha_g}, \tag{66}$$

$$p_{n+1} = \frac{p_n + \alpha_p \Delta s_{\mathrm{M}n}}{1 + \alpha_p \Delta s_{\mathrm{M}n}}, \tag{67}$$

$$\mathbf{T}^{\mathrm{h}}_{n+1} = \frac{\mathbf{T}^{\mathrm{h}}_n + c(p_{n+1}, g_{n+1})\mathbf{D}\Delta\mathbf{E}_n}{1 + b\Delta s_{\mathrm{M}n}}, \tag{68}$$

$$\mathbf{E}_{\mathrm{v}n+1} = \frac{\mathbf{E}_{\mathrm{v}n}\eta(\mathbf{E}_{\mathrm{M}n+1}) + 2\Delta t_n G_{\mathrm{ov}}(p_{n+1})\mathbf{D}\mathbf{E}_{n+1}}{\eta(\mathbf{E}_{\mathrm{M}n+1}) + 2\Delta t_n G_{\mathrm{ov}}(p_{n+1})}. \tag{69}$$

equation (66) is obtained for the positive solution of the quadratic equation for g_{n+1}, which results from (62). The functions for the material parameters are given by

$$c(p_{n+1}, g_{n+1}) = \frac{c_1(1 - c_2 \exp(c_3 g))}{p_{n+1} + 1}, \tag{70}$$

$$G_{\mathrm{ov}}(p_{n+1}) = G_1(1 - p_{n+1})^{r_{\mathrm{ov}}} + G_2, \tag{71}$$

$$\eta(\mathbf{E}_{\mathrm{M}n+1}) = \eta_0 \left(\left(\frac{1}{s_\eta} \frac{\Delta s_{\mathrm{M}n}(\mathbf{E}_{\mathrm{M}n+1})}{\Delta t_n} + \alpha_\eta \right)^{-r_\eta} + 1 \right). \tag{72}$$

Now, the total stress can be calculated by

$$\mathbf{T}_{n+1} = \mathbf{T}_{\mathrm{eq}n+1} + \mathbf{T}_{\mathrm{ov}n+1} \tag{73}$$

with the equilibrium stress

$$\mathbf{T}_{\mathrm{eq}n+1} = K_{\mathrm{eq}}(\mathrm{tr}\,\mathbf{E}_{n+1})\mathbf{I} + 2G_{\mathrm{eq}}\mathbf{D}\mathbf{E}_{n+1} + \mathbf{T}^{\mathrm{h}}_{n+1}, \tag{74}$$

and the overstress

$$\mathbf{T}_{\mathrm{ov}n+1} = 2G_{\mathrm{ov}}(p_{n+1})\mathbf{D}(\mathbf{E}_{\mathrm{M}n+1} - \mathbf{E}_{\mathrm{v}n+1}). \tag{75}$$

With the simplification of equation (25) in the implementation, we obtain a model, where the internal variables can be calculated without a local Newton iteration, which is an advantage from the point of view of computational efficiency.

5.1 Simulation Example

In this section, the behavior of the model is demonstrated with a numerical example. In this example, we consider a complex geometry modeled with the proposed material. The geometry, mesh and boundary conditions are shown in Figure 10.

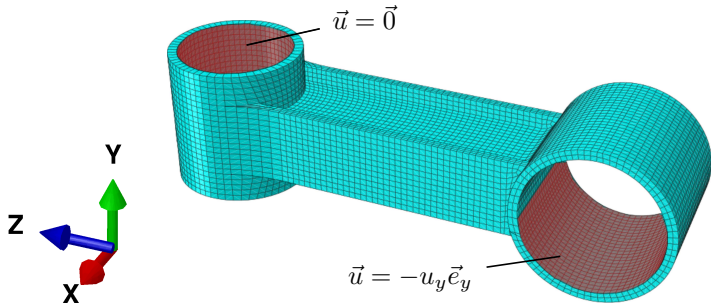

Figure 10. Mesh and boundary condition

The part is fixed in left red area and we apply a displacement in negative y-direction u_y with a constant displacement rate in the right red area. Two different displacement rates are investigated, $\dot{u}_1 = 2 \times 10^{-1}\,\mathrm{mms}^{-1}$ and $\dot{u}_2 = 2 \times 10^{-3}\,\mathrm{mms}^{-1}$, and three different aging times: without aging, with 6 months aging and with 2 years aging. The mesh is composed of 11 783 twenty-noded hexahedral elements. The time step for the simulations is

chosen as $\Delta t_1 = 0.33\,\mathrm{s}$ for the first displacement rate and $\Delta t_2 = 10\,\mathrm{s}$ for the second one. For the simulations, the initial conditions are for the component without aging $g(0) = 0$, for six months aging $g(0) = 0.637$ and for two years $g(0) = 0.933$, with $t = 0$ the initial time of the simulation. During the simulations, the aging variable changes its value marginally, since the aging happens more slowly than the deformation process.

The results of the simulations are shown in Figures 11 and 12. Figure 11 shows the reaction force for the six different cases. In this diagram, it becomes clear that rate dependence as well as the aging stage of the material exhibit a strong influence on the mechanical response. Here, we observe a reduction in the reaction force of approximately 20% between the unaged material at the fast displacement rate and the material after two years aging at the slow displacement rate. Figure 12 displays the von Mises stress for the unaged material at the fast

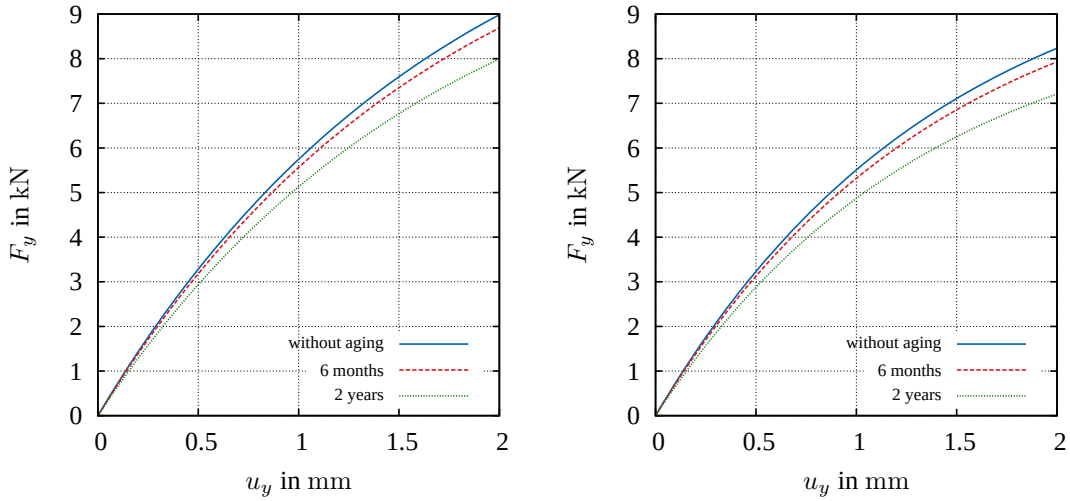

(a) Fast displacement rate $\dot{u}_1$

(b) Slow displacement rate $\dot{u}_2$

Figure 11. Reaction force over the displacement for the different aging times and displacement rates

displacement rate, the 2-years aged material at the fast displacement rate and at the slow displacement rate. Here, we observe again a reduction in the von Mises stress of 11% for the same displacement rate but with two different aging times (Sim. 1 and Sim. 2) and a reduction of 18% with the same aging stage for two different displacement rates (Sim. 2 and Sim. 3).

6 Conclusion

In this work, the influence of aging on the mechanical response of the zinc die-casting alloy zamak 5 has been investigated. Experiments at different strain rates for tension, compression and torsion were carried out with the help of thin-walled cylindrical specimens. Additionally, the specimens were investigated at different ages in order to gather data of the alteration of the material behavior over the time. Since the material belongs to the material class of viscoplasticity, relaxation and multi step tests have been carried out to describe the equilibrium hysteresis. The developed material model is motivated by a rheological model where the stresses are decomposed into an equilibrium part and an overstress part. With the help of an internal variable g, the influence of aging is introduced in the model. Furthermore, the thermomechanical consistence of the model is shown. The material parameters of the model are identified using an approach where the different phenomena are addressed consequently making use of the partitioned structure of the model. The identification is carried out mainly for the shear behavior of the model, leading to a good agreement in tension and compression, where just one parameter was identified. Finally, we observe the influence of aging and strain rate in the computed reaction force and von Mises stress in a simulation example, which differs in this concrete example in about 20%, and which shows the importance of considering these effects in the prediction for components made of zamak 5.

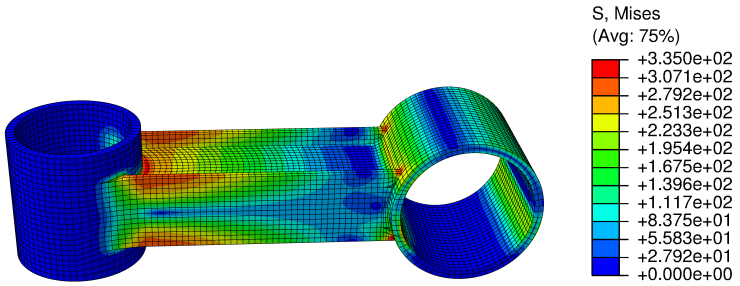

(a) Sim. 1: without aging, $\dot{u}_1 = 2 \times 10^{-1}\,\mathrm{mms}^{-1}$

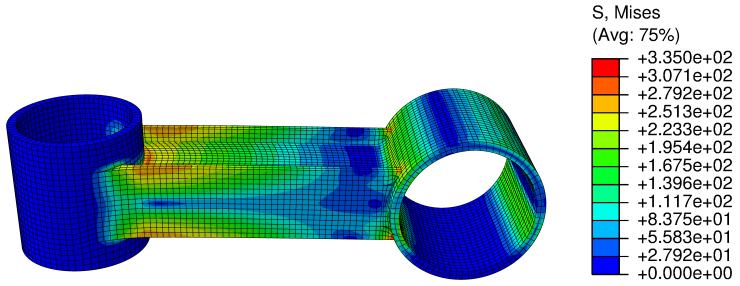

(b) Sim. 2: two years aging, $\dot{u}_1 = 2 \times 10^{-1}\,\mathrm{mms}^{-1}$

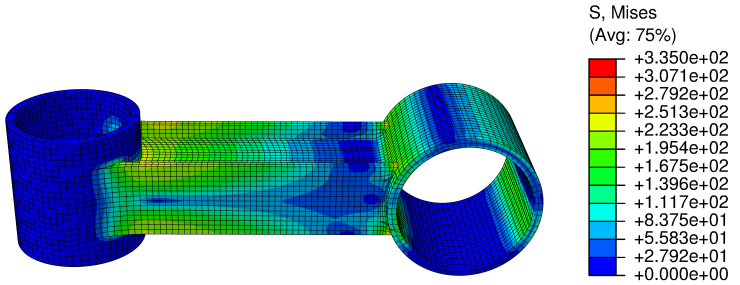

(c) Sim. 3: two years aging, $\dot{u}_2 = 2 \times 10^{-3}\,\mathrm{mms}^{-1}$

Figure 12. Von Mises stress in MPa for three different cases

Acknowledgments:

We would like to thank the German Research Foundation DFG for funding this research project with the project no. DFG HA2024-18/1.

References

Bazant, Z. P.; Huet, C.: Thermodynamic functions for ageing viscoelasicity: integral form wihout internal variables. *International Journal of Solids and Structures*, 36, (1999), 3993–4016.

Callister, W. D.; Rethwisch, D.: *Fundamentals of materials science and engineering*. Wiley (2016).

Carol, I.; Bazant, Z.: Viscoplasticity with aging caused by solidification of nonaging constituent. *Journal of Engineering Mechanics*, 119, (1993), 2252–2269.

Dippel, B.; Johlitz, M.; Lion, A.: Ageing of polymer bonds: a coupled chemomechanical modelling approach. *Continuum Mechanics and Thermodynamics*, 26, (2014), 247–257.

Gebhard, E.: Die Zinkecke des Dreistoffsystems Zink-Aluminium-Kupfer. *Zeitschrift für Metallkunde*, 32, 4, (1940), 78–85.

Gebhard, E.: Über den β-Zerfall in aluminiumhaltigen Zinklegierungen und den Einfluss kleiner Beimengungen auf die Zerfallsgeschwindigkeit. *Zeitschrift für Metallkunde*, 33, 8/9, (1941), 328–332.

Gebhard, E.: Über den Aufbau und die Volumenänderung der Zink-Kupfer-Aluminium-Legierungen. *Zeitschrift für Metallkunde*, 34, 9, (1942), 208–215.

Hartmann, S.: A thermomechanically consistent constitutive model for polyoxymethylene: experiments, material modeling and computation. *Archive of Applied Mechanics*, 76, (2006), 349–366.

Haupt, P.: *Continuum Mechanics and Theory of Materials*. Springer Verlag, Berlin (2000).

Haupt, P.; Lion, A.: Experimental identification and mathematical modelling of viscoplastic material behavior. *Journal of Continuum Mechanics and Thermodynamics*, 7, (1995), 73–96.

Haupt, P.; Sedlan, K.: Viscoplasticity of elastomeric materials. experimental facts and constitutive modelling. *Archive of Applied Mechanics*, 71, (2001), 89–109.

Johlitz, M.: On the representation of ageing phenomena. *The Journal of Adhesion*, 88, (2012), 620–648.

Johlitz, M.; Diercks, A., Nico ans Lion: Thermo-oxidative ageing of elastomers: A modelling approach based on a finite strain theory. *International Journal of Plasticity*, 63, (2014), 138–151.

Johlitz, M.; Lion, A.: Chemo-thermomechanical ageing of elastomers based on multiphase continuum mechanics. *Continuum Mechanics and Thermodynamics*, 25, (2013), 605–624.

Johnen, H. J.: *Zink-Taschenbuch*. Metall-Verlag (1981).

Kallien, L. H.; Busse, M.: Ursachen und Möglichkeiten zur Minimierung der Alterungsvorgänge bei Zinkdruckgusslegierungen. Tech. rep., Hochschule Aalen and IFAM Bremen (2009).

Krämer, S.; Rothe, S.; Hartmann, S.: Homogeneous stress-strain states computed by 3D-stress algorithms of FE-codes: applications to material parameter identification. *Engineering with Computers*, 31, (2015), 141–159.

Krempl, E.: Viscoplasticity based on total strain. the modelling of creep with special considerations on initial strain and aging. *Journal of Engineering Materials and Technology*, 101, (1979), 380–386.

Leis, W.; Kallien, L. H.: Ageing of zink alloys. *International Foundry Research*, 64, 1, (2011), 2–23.

Lion, A.; Dippel, B.; Liebl, C.: Thermomechanical material modelling based on a hybrid free energy density depending on pressure, isochoric deformation and temperature. *International Journal of Solids and Structures*, 51, (2014), 729–739.

Lion, A.; Johlitz, M.: On the representation of chemical ageing of rubber in continuum mechanics. *International Journal of Solids and Structures*, 49, (2012), 1227–1240.

Maghous, S.; Creus, G.: Periodic homogenization in thermoviscoelasticity: case of multilayered media with ageing. *International Journal of Solids and Structures*, 40, (2003), 851–870.

Marquis, D.; Costa Mattos, H.: Modeling of plasticity and aging as coupled phenomena. *International Journal of Plasticity*, 7, (1991), 865–877.

Marquis, D.; Lemaitre, J.: Constitutive equations for the coupling between elasto-plasticity damage and aging. *Revue de Physique Applique*, 23, (1988), 615–624.

Meschke, G.: Consideration of aging of shotcrete in the context of a 3D viscoplastic material model. *International Journal for Numerical Methods in Engineering*, 39, (1996), 3123–3143.

Murray, J.: The Al-Zn (aluminium-zinc) system. *B. Alloy Phase Diagrams*, 4, (1983), 55–73.

Zhu, Y.: Phase transformations of eutectoid Zn-Al alloys. *Journal of Materials Science*, 36, (2001), 3973–3980.

Zhu, Y.: General rule of phase decomposition in Zn-Al based alloys (II) – on effects of external stresses on phase transformations –. *Material Transactions*, 45, 11, (2004), 3083–3097.

Zhu, Y.; Hinojosa, J.; Yue, T.; Lee, W.: Structural evolution in a continuously cast eutectoid Zn-Al-based alloy. *Materials Characterization*, 48, (2002), 315–322.

Zhu, Y.; Man, H.; Dorantes-Rosales, H.; Lee, W.: Ageing characteristics of furnace cooled eutectoid Zn-Al based alloys. *Journal of Materials Science*, 38, (2003), 2925–2934.

Address: Institute of Applied Mechanics, Clausthal University of Technology, Adolph-Roemer-Str. 2a, 38678 Clausthal-Zellerfeld, Germany
email: maria.angeles.martinez.page@tu-clausthal.de, stefan.hartmann@tu-clausthal.de